

MODELING SEISMICITY RATE CHANGES ALONG THE HELLENIC SUBDUCTION ZONE (GREECE)

Leptokaropoulos K. M.¹, Papadimitriou E. E.¹, Orlecka-Sikora B.²
Karakostas V. G.³ and Vallianatos F.³

¹Geophysics Department, School of Geology, Aristotle University of Thessaloniki, GR54124
Thessaloniki, kleptoka@geo.auth.gr, ritsa@geo.auth.gr, vkarak@geo.auth.gr

²Seismology and Physics of the Earth's Interior, Institute of Geophysics, Polish Academy of Sciences, Warsaw, Poland, orlecka@igf.edu.pl

³Laboratory of Geophysics and Seismology, Technological Educational Institute of Crete,
fvallian@chania.teicrete.gr

Abstract

The Dieterich (1994) Rate/State formulation was applied for the seismicity rate changes in the western part of the Hellenic arc to be investigated. The completeness magnitude of the shallow seismicity ($h < 60\text{km}$) was firstly evaluated for different time windows. The spatio-temporal changes of these seismicity rates (reference rates) were studied then for the interevent periods between successive strong ($M \geq 6.0$) earthquakes. These changes were correlated with the Coulomb stress changes (ΔCFF) produced by the stronger events, through a Rate/State model which incorporates physical parameters associated with fault dynamics such as the tectonic stressing rate, fault constitutive parameters and frictional response of the rupture zones. The influence of the former parameters in the model performance was tested by evaluating the linear correlation coefficient between modeled and real earthquake production rates along with their confidence limits. Application of different parameter values was attempted for the sensitivity of the calculated seismicity rates and their fit to the real data to be tested. Given the geographical peculiarity of the Hellenic Subduction zone, that yields to high uncertainties in the earthquake focal parameter determination, the results demonstrate that the present formulation and the available data sets are sufficient enough to contribute to a robust seismic hazard assessment.

Key words: Coulomb stress changes, Rate/state stress transfer, smoothed seismicity.

Περίληψη

Οι μεταβολές των ρυθμών σεισμικότητας στο δυτικό τμήμα του Ελληνικού Τόξου μελετήθηκαν με βάση το μοντέλο Ρυθμού/Κατάστασης (Dieterich, 1994). Καθορίστηκε το μέγεθος πληρότητας των καταλόγου επιφανειακών σεισμών ($h < 60\text{km}$) για διαφορετικά χρονικά διαστήματα και έγινε μελέτη των μεταβολών των ρυθμών σεισμικότητας αναφοράς στο χώρο και το χρόνο για τις περιόδους μεταξύ διαδοχικών ισχυρών ($M \geq 6.0$) σεισμών. Οι μεταβολές αυτές συνχετίσθηκαν με τις μεταβολές των στατικών τάσεων Coulomb (ΔCFF), που συνδέονται με τη γένεση των ισχυρών σεισμών, σε ένα μοντέλο που συνδυάζει φυσικές παραμέτρους των ρηγμάτων όπως οι ρυθμοί τεκτονικής φόρτισης, οι καταστατικές παράμετροι και η τριβή. Η επίδραση των

τιμών αυτών των παραμέτρων εκτιμήθηκε με τον υπολογισμό του συντελεστή γραμμικής συσχέτισης μεταξύ των πραγματικών και των υπολογισμένων με βάση το μοντέλο ρυθμών σεισμικότητας και τον διαστήματος εμπιστοσύνης του. Εφαρμόστηκαν διαφορετικές τιμές των παραμέτρων που υπεισέρχονται στο μοντέλο για να ελεγχθεί η εναισθησία υπολογισμού των εκτιμώμενων ρυθμών στη διακύμανση των τιμών αντών. Με δεδομένη την γεωγραφική ιδιαιτερότητα της περιοχής μελέτης, εξαιτίας της οποίας προκύπτουν σημαντικές αβεβαιότητες στον προσδιορισμό των εστιακών παραμέτρων των σεισμών, τα αποτελέσματα της εργασίας δείχνουν ότι η συγκεκριμένη μεθοδολογία και τα διαθέσιμα δεδομένα μπορούν να προσφέρουν μια αξιόπιστη εκτίμηση σεισμικής επικινδυνότητας.

Λέξεις κλειδιά: Μεταβολές Τάσεων Coulomb, Μοντέλο Ρυθμού/Κατάστασης, Ομαλοποιημένη Σεισμικότητα.

1. Introduction

The Hellenic subduction zone (Figure 1) constitutes one of the most rapidly deforming parts of the Alpine-Himalayan mountain belt, exhibiting intense shallow and intermediate depth seismic activity and experiencing several devastating earthquakes known from both historical reports and instrumental recordings. The strongest earthquake that ever occurred in the broader Aegean region, was located at the southwestern part of the Hellenic Arc, near Crete Island (M8.3), in AD 365 (Papazachos & Papazachou, 2003; Papadimitriou & Karakostas, 2008; Shaw, 2012). The subduction thrust belt is the most prominent feature of the broader Aegean region between the slowly converging Eastern Mediterranean oceanic lithosphere and Aegean microplate with a well constrained, from GPS data and the geological history, rate of convergence of about 4cm/yr (Clarke et al., 1998; McClusky et al., 2000). This deformation rate is enough to induce a roll-back at the Hellenic Trench leading to significant extension of the overriding plate with the back-arc

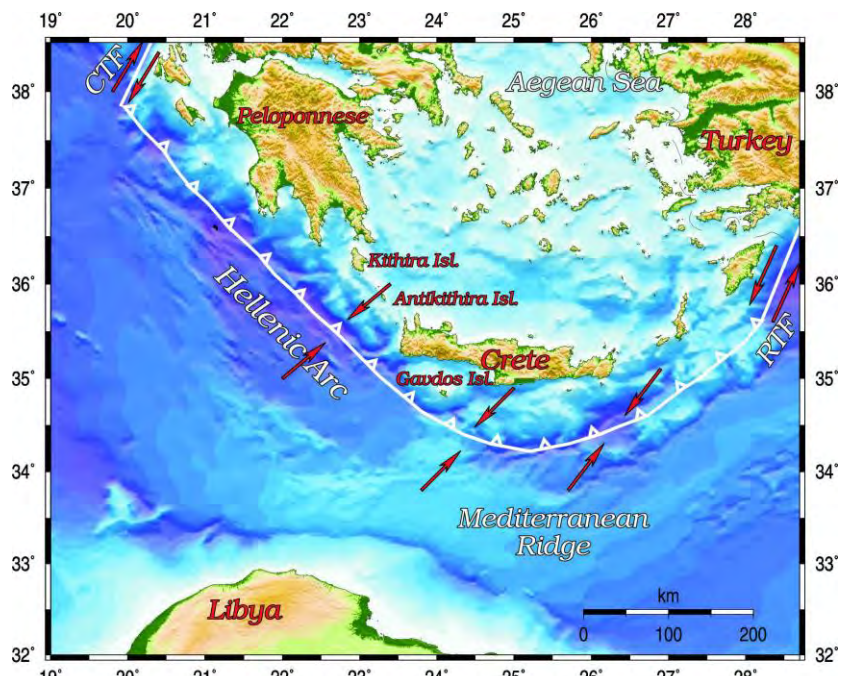


Figure 1 - Morphology and main seismotectonic properties of the study area (Papadimitriou & Karakostas, 2008).

stretching direction being oblique to the trench roll-back direction. This zone is extended between the two Subduction-Transform Edge Propagators (STEP) of the dextral Cephalonia Transform Fault in the west (Scordilis et al., 1985) and the sinistral Rhodos fault in the east (Papazachos and Papazachou, 2003) over a distance of approximately 1000km.

The existence of a Wadati-Benioff zone which is dipping about 30° at its shallow segment until 100km depth and then descending with a steeper angle of 45° was first recognized by Papazachos & Comninakis (1971) and it was then confirmed from seismic hypocenter studies (Hatzfeld and Martin, 1992; Papazachos et al., 2000). Seismic tomography revealed the deeper branches of subducted lithosphere at a depth of 600 km (Spakman et al. 1988, Papazachos and Nolet 1997).

Seismic deformation is not uniformly distributed throughout the region as the tectonic structures are related to complex tectonic evolution and deformation patterns. Both extensional and compressive regimes are evident in the region (Taymaz et al., 1990, 1991; Papazachos & Kiratzi, 1996; Benetatos et al., 2004; Yolsal-Çevikbilen & Taymaz, 2012) resulted to three major faulting types. The shallow earthquakes in the external part of the subduction system are associated with low angle, reverse faulting with the P-axis being almost perpendicular to the subduction front. This latter seismic activity is responsible for the most destructive earthquakes throughout the entire Arc. The second type involves crustal earthquakes in a backarc narrow extensional continental zone with the T-Axis orientated in an almost east-west direction and faults striking almost N-S running parallel to the arc (Papazachos et al., 1998; Benetatos et al., 2004). The intermediate depth events occur onto the descending slab and are associated with strike slip faulting with a considerable thrust component, with maximum tension trending parallel to the dip of the Wadati–Benioff zone and maximum compression being almost horizontal and parallel to the arc direction (Kiratzi and Papazachos 1995, Papazachos 1996). Normal faulting with E-W orientated strike dominate the backarc region.

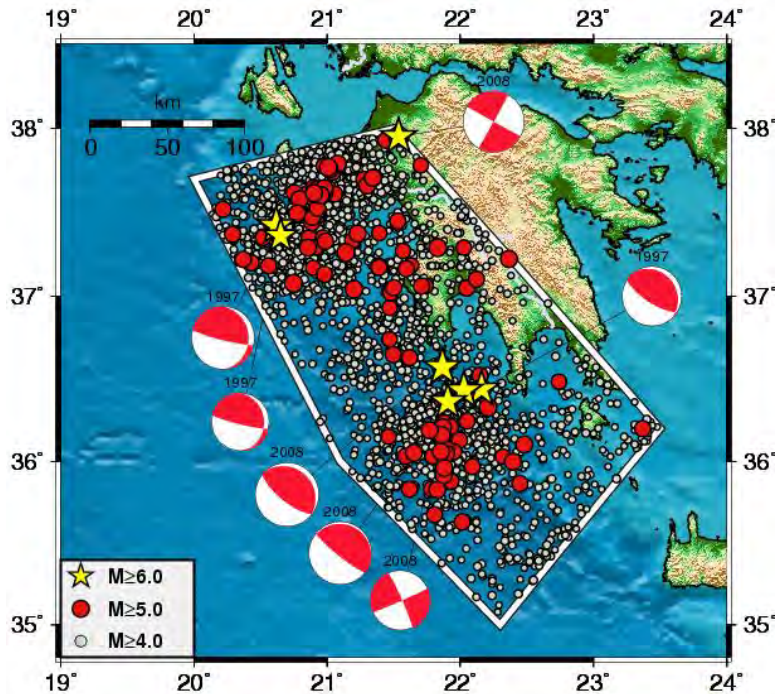


Figure 2 – Earthquake ($M \geq 6.0$) fault plane solutions that occurred in the study area since 1997, shown as lower hemisphere equal area projections. Epicenters of the earthquakes with $M \geq 4.0$ since 1971 are also depicted. Information about these strong events is also given in Table 1.

2. Method

The evaluation of seismicity rate changes in terms of Coulomb static stress changes is performed on the basis of a Rate/State model, proposed by Dieterich (1994). According to Rate/State stress transfer concept, a sudden positive stress step, results to an immediate increase of the seismicity rate, which is temporary and attenuates with time following the Omori's decay law. Similarly, a sudden stress drop brings on a seismicity rate decrease, which also tends to recover with time to the initial rate, due to the effect of the stressing rate (constant or variable). These rate changes can be observed either along the fault, which caused the main shock (along fault aftershocks), or in nearby faults (off-fault triggering) up to a distance proportional to the final slip distribution regardless the dynamics of the rupture (Gomberg et al., 2005). Applications of the model (e. g. Toda et al., 1998; Toda et al., 2005; Catalli et al., 2008) have shown that seismicity rate changes, R , strongly depend on clock-advanced failure, the fault stressing rate, $\dot{\tau}$, and the reference rates of earthquake production, r , expressed as:

$$R = \frac{r}{\gamma \cdot \dot{\tau}_r} \quad (1)$$

Where γ , is the state variable for seismicity formulation that evolves with time and stressing history and alters its value because of the stress perturbations, causing seismicity rate changes. The seismicity rate equation, as a function of time, t , has the form (Dieterich & Kilgore, 1996):

$$R(t) = \frac{r}{\left[\exp\left(\frac{-\Delta CFF}{A\sigma}\right) - 1 \right] \exp\left(\frac{-t}{t_a}\right) + 1} \quad (2)$$

Here, t_a , is the characteristic relaxation time for the perturbation of earthquake rate, A is a fault constitutive parameter, σ is the total normal stress and ΔCFF is the coseismic Coulomb stress changes, given by $\Delta CFF = \Delta\tau + \mu' \Delta\sigma_n$, with $\Delta\tau$, being shear stress change, $\Delta\sigma_n$, stands for the normal stress change and μ' , the apparent coefficient of friction, including pore pressure effects (Simpson and Reasenberg, 1994). Product $A\sigma$, describes the instantaneous response of friction to a step change in slip speed (Toda & Stein, 2003). Reference and observed seismicity rates for any inter-event time interval are computed by spatially smoothing the seismicity. For this purpose we use a probability density function (PDF) of epicenters distribution. This function determines the seismicity rates at the center of each cell of a normal grid superimposed on the study area and these values are considered constant in time as the same is considered for the secular tectonic stressing rate. The PDF is estimated by a bivariate kernel density estimator of the form (Silverman, 1986):

$$f(x, y) = \frac{1}{nh^2} \sum_{i=1}^n K\left(\frac{x - X_i}{h}, \frac{y - Y_i}{h}\right) \quad (3)$$

Where K stands for the Gaussian Kernel of the form:

$$K(x, y) = \frac{1}{2\pi} e^{-\frac{(x^2+y^2)}{2}} \quad (4)$$

Where X_i , Y_i , are the epicentral coordinates of earthquakes (longitude, λ and latitude, ϕ , respectively), x , y , are the coordinates of the centers of the bins, on which the PDF value is going to be estimated, n , is the number of the events and h , is the smoothing parameter (or window width), having the same units with X_i , Y_i , x , y . The kernel determines the regularity and the shape of the estimator, whereas the window width controls the degree of smoothing. From equations (3) and (4) the probability is derived:

$$P = \frac{1}{4n} \sum_{i=1}^n [erf(\frac{y_2 - Y_i}{h\sqrt{2}}) \cdot (erf(\frac{-x_1 + X_i}{h\sqrt{2}}) - erf(\frac{-x_2 + X_i}{h\sqrt{2}})) + erf(\frac{y_1 - Y_i}{h\sqrt{2}}) \cdot (erf(\frac{-x_2 + X_i}{h\sqrt{2}}) - erf(\frac{-x_1 + X_i}{h\sqrt{2}}))] \quad (5)$$

$$\text{With } erf(x) = \frac{2}{\sqrt{\pi}} \int_0^x e^{-t^2} dt \quad (6)$$

which is twice the integral of the Gaussian distribution with mean zero and variance of 1/2. Finally the seismicity rate is estimated for the given time period, Δt as, $R=n/\Delta t$. This corresponds to the real seismicity rate of the given time period and is compared with the value of expected seismicity rate for the respective period resulted from (2).

2.1 Data Selection

We selected the shallow seismicity ($h < 60$ km) data in the western part of the Hellenic arc between the Kephalonia transform fault and Crete Island, since 1970. Then the completeness magnitude, M_c , was evaluated for different time increments with the methodology of Leptokaropoulos et al. (2012) as shown in Table 1. In each case two different periods with different duration and M_c were considered to calculate the reference seismicity rates. These periods were selected for data sufficiency and longest possible duration to be achieved.

Table 1 – Magnitude of completeness as calculated for different periods

Period		Period	Mc	Period	Mc
1971-1980	4.0	1991-2000	3.6	2001-2007	3.6
1981-1990	3.7	2001-2012	3.6	2008-2012	3.5

2.2 ΔCFF Calculations

Coulomb stress changes were calculated from the coseismic displacements of the stronger ($M \geq 6.0$) events (Table 2) that occurred in the study areas since 1996. Fault lengths, L, were determined following the spatial distribution of the stronger, well located aftershocks. The respective widths were estimated from the dip angle of the fault and the distance measured down-dip from the surface to the upper and lower edges of the rectangular dislocation plane, respectively, as $h/\sin(\text{dip})$, where H , is the width of the seismogenic layer (3 – 20km). For the low angle dipping faults the constraint $L \geq W$ was set. The mean coseismic slip, u , was calculated from the seismic moment, M_o , of an earthquake, as $M_o = G \cdot u \cdot L \cdot w$, where, G , stands for the shear modulus and equals to $3.3 \cdot 10^5$ bars. All ΔCFF calculations were done at the depth of 8km, which represents approximately the nucleation depth. The calculation of the stress field changes was done according to the representative fault plane geometry and sense of slip as found for each one of the study sub-areas. The apparent coefficient of friction, μ' , and the Poisson ration, v , were considered equal to 0.4 and 0.25, respectively.

Table 2 – Source mechanisms of the events considered in this study.

Year	Date	Lat(oN)	Lon(oE)	h(km)	M	strike	dip	rake	Reference
1997	13OCT	36.440	22.160	13.0	6.3	123	72	84	Kiratzi & Louvari, 2003
1997	18NOV	37.420	20.619	10.0	6.6	354	20	159	
1997	18NOV	37.360	20.650	5.0	6.1	354	20	159	
2008	14FEB	36.570	21.868	20.0	6.7	312	18	93	
2008	14FEB	36.430	22.026	8.6	6.6	292	8	74	GCMT
2008	20FEB	36.360	21.907	9.4	6.3	336	85	178	
2008	8JUN	37.950	21.537	15.0	6.4	301	74	7	

2.3 Expected Seismicity Rates – Rate/State Parameters

The expected seismicity rates were therefore calculated in each cell from eq. 2, given the reference seismicity rate, r , the static Coulomb stress changes, ΔCFF , the characteristic relaxation time, t_a , which was considered to range between 2.5yr-25yrs and the product $A\sigma$ (fault constitutive parameter, A , total normal stress, σ). This product is connected with the characteristic time and the long term tectonic loading, τ_r , as $A\sigma = \tau_r \cdot t_a$. The tectonic loading was selected ranging from 0.005bar/yr to 0.06bar/yr. The aforementioned values of t_a and τ_r , lead to an $A\sigma$ ranging from 0.0125 – 1.5 bars.

3. Qualitative and Quantitative Analysis

Once the modeled seismicity rates are calculated, they are compared with the observed ones for the respective time windows. A qualitative fitting was accomplished by comparison of the patterns of observed and expected seismicity and the locations of the events that occurred during the respective periods and for specific parameter values (Figure 3). One more qualitative representation was done by mapping the ratio of expected/observed seismicity rates in the study areas (Figure 4). Thus, the declination of the modeled from the real values becomes more evident. Quantitative comparison was done by calculation of the Pearson's linear correlation coefficient (PCC) and its 95% confidence intervals (Figure 5). Significance testing for PCC was also performed by estimating the corresponding p-value that is the highest level of significance at which the null hypothesis stating that $PCC=0$ can still be rejected.

The influence of 7 strong events (3 in 1997 and 4 in 2008) was taken into consideration to calculate ΔCFF and to model expected seismicity rates (Figure 3). The reference seismicity rate was calculated for 1971-1997 ($M_c=4.0$). The June 2008 event occurred outside the area borders but it was close enough to alter the regional stress field. In the first period (1997-2008) the correlation is much stronger, especially in the central and northern part of the area. The second period (2008-2012) is not long enough to contain sufficient data and therefore the correlation coefficient is relatively low ($h=0.08^\circ$, $t_a=10$ yrs, $\tau_r=0.01$ bar/yr). Similar results for the first period yielded when reference seismicity rates were calculated from 1981-1997 ($M_c=3.7$), although they were somewhat amplified in comparison with the previous approach, because in this period the dataset contains a larger number of events (smaller M_c). For the second period, more events are available, but the correlation does not show any improvement with a significant number of earthquakes taking place in stress shadows.

The ratio of expected/observed seismicity rate for the two study periods is shown in Figure 4 with calculations done considering reference seismicity rate evaluated for 1981-1997 ($M_c=3.7$). The ratio is close to 1 for the first period but it diverges to higher values for the second one, indicating that the modeled rates are higher than the expected ones ($h=0.08^\circ$, $t_a=10$ yrs, $\tau_r=0.01$ bar/yr). The patterns are similar if we consider reference seismicity rate calculated for 1971-1997, but here are more obvious in the second period (2008-2012) due to larger sample available.

The quantitative analysis shows that there is a relatively high correlation between observed and modelled seismicity rates for the first of the study periods. This correlation is even stronger in areas experiencing positive ΔCFF values and reaches over 70% in most of the cases. For the time interval from February to June 2008, there is no correlation at all (~ 0) because of the very small span of the time window resulted to shortage of data. Finally, for the period 2008-2012 a moderate correlation is evident which become higher for positive ΔCFF areas. This happens due to the fact that the catalog is dominated by along-fault aftershocks, that took place in the close vicinity of the faults segment connected with these main events. Therefore, it is very likely that the correlation will be improved as time passes and the aftershock sequence decay at the reference rate.

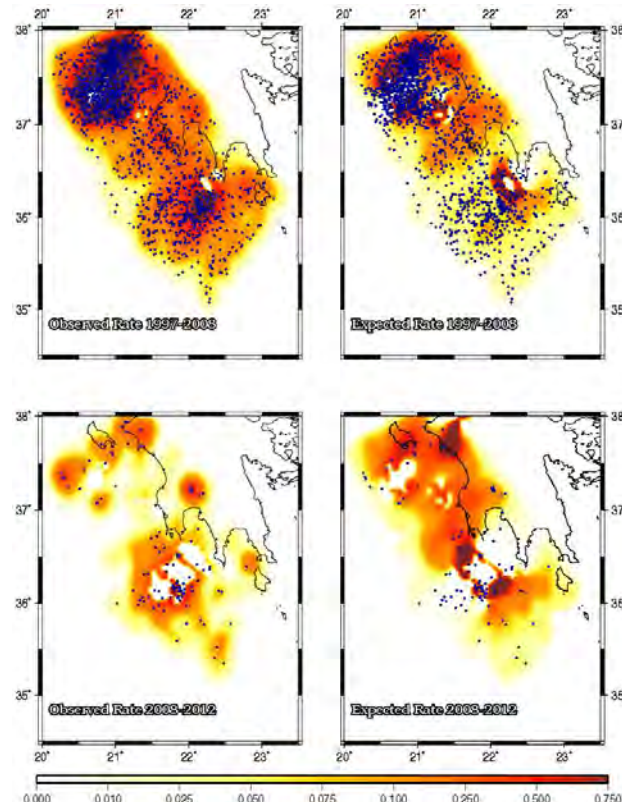


Figure 3 – Observed (left frames) and modelled (right frames) seismicity rates. Blue dots represent the epicentres of the earthquakes occurred during the respective periods. The reference seismicity rate was calculated during 1971-1997 ($M \geq 4.0$).

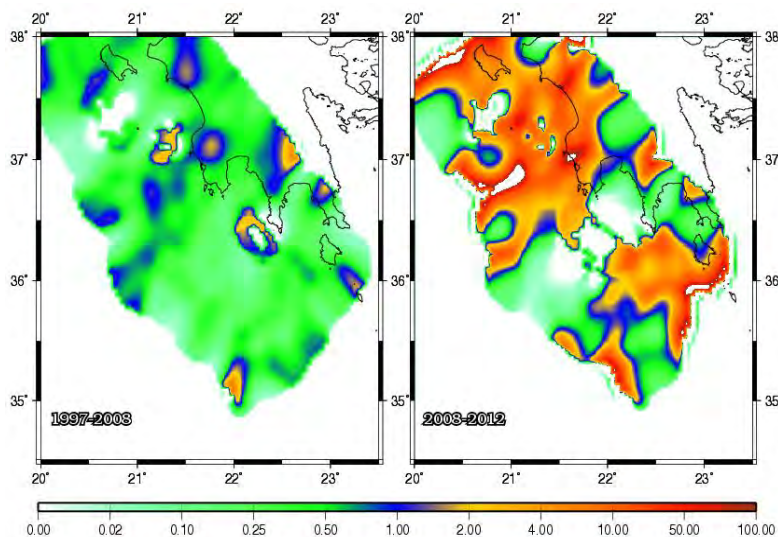


Figure 4 - Ratio of expected/observed seismicity rates for the inter event periods. Green colors indicate regions where expected seismicity rates are lower than the observed ones while warmer colors stand for regions with higher expected rates in comparison with the observed ones. Applied parameter values were: $h=0.08^\circ$, $t_a=10$ yrs, $\tau_r=0.01$ bar/yr, $A\sigma=0.1$ bar. Reference seismicity rate was considered from the period 1981-1997 ($M \geq 3.7$).

4. Discussion and Conclusion

In the application of the Dieterich (1994) rate/state model, we started with a “learning period” (either 1971-1997 or 1981-1997) and a reference seismicity rate was then evaluated. The static Coulomb stress changes (ΔCFF), caused by strong earthquakes’ occurrence were calculated and their influence to the reference seismicity rates were estimated. The impact of the constant tectonic loading (stressing rate) during the inter-seismic periods (or ‘testing periods’) was embodied to the modeled seismic rates. Summarizing, the simulated earthquake occurrence rates were estimated as a result of the effect of the successive coseismic ΔCFF and the steady-rate tectonic loading on the reference rates evaluated from the learning period’s seismicity. These calculations are performed just before and after a strong earthquake takes place, and therefore the real (observed) seismicity rates during the inter-event periods are also evaluated (following the same procedure as with the reference seismicity rates). The results are qualitatively and quantitatively compared with the modeled ones in order to seek for correlation between observed-expected seismic rates and improve the modeling by selection/combinations of parameter values applied.

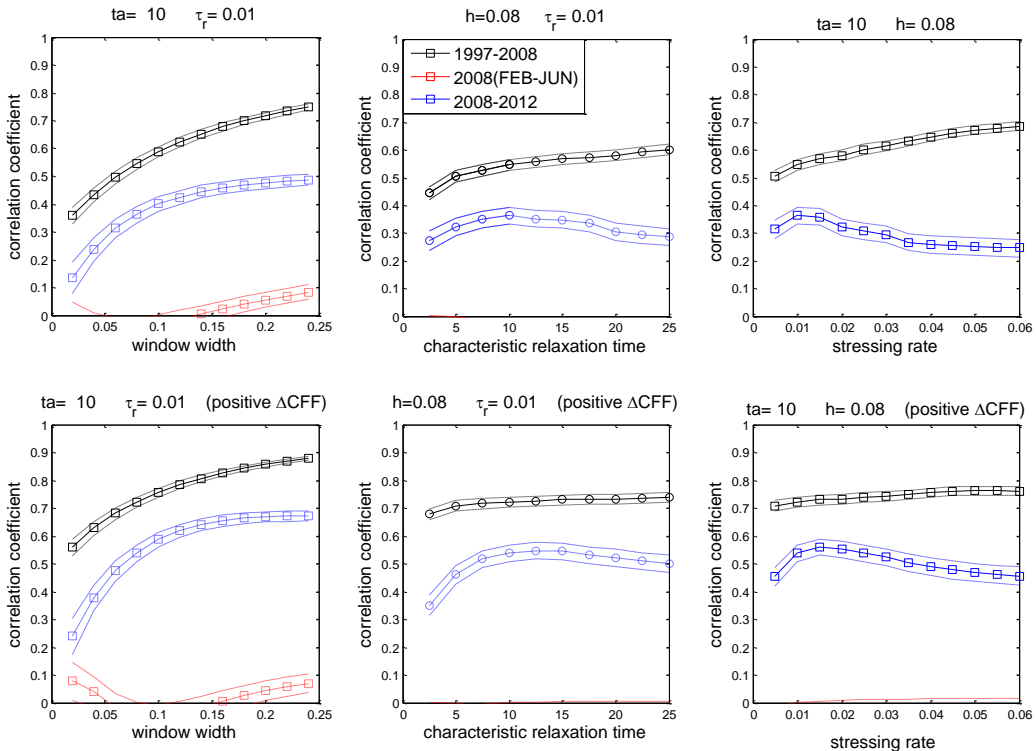


Figure 5 - Quantitative evaluation of the difference between observed-synthetic seismicity rates during the inter-event time periods (colored lines). Solid lines indicate the value of Pearson linear Correlation Coefficient (PCC) while dashed lines indicate its lower and upper bounds for a 95% confidence interval for each coefficient. The upper frame figure yielded from the whole data, while the figure below by taking into account only those cells which experience positive ΔCFF .

The results indicate that the correlation between observed and simulated seismicity rate values is quite high when the study periods last enough for the respective dataset exhibiting sufficient size and including adequate number of off-fault earthquakes. In some of the cases the expected rates are very close to the observed ones, whereas, in the remaining cases the model tends to overestimate the seismicity rates in comparison with the real ones, although the spatial distribution

of expected seismicity rates fits well to the observed one. When a different learning period was considered in order to obtain bigger sample, both qualitative and quantitative correlation was slightly improved. When cells experience positive ΔCFF are only considered in the calculations, stronger correlation is obtained. Even if several assumptions were taken into consideration (uniform stressing rate, ΔCFF calculation according to a specific type of faulting, influence of strong events before 1997 was not considered), the results show that successful modeling seismicity rate changes through this approach is feasible. Implication of the current analysis to earthquake probabilities is expected to significantly contribute to time dependent seismic hazard assessment. Given a magnitude frequency relation the rates of the strongest events occurrence can be easily transformed to probability of earthquake occurrence

5. Acknowledgments

This work was supported by the THALES Program of the Ministry of Education of Greece and the European Union in the framework of the project entitled "Integrated understanding of Seismicity, using innovative Methodologies of Fracture mechanics along with Earthquake and non extensive statistical physics – Application to the geodynamic system of the Hellenic Arc. SEISMO FEAR HELLARC". The GMT system (Wessel and Smith, 1998) was used to plot some of the figures. Geophysics Department, AUTH, contribution number 814.

6. References

- Benetatos C., Kiratzi A., Papazachos C. and Karakaisis G. 2004. Focal mechanisms of shallow and intermediate depth earthquakes along the Hellenic Arc, *J. Geodyn.*, 37, 253-296.
- Catalli F., Cocco M., Console R. and Chiaraluce L. 2008. Modeling seismicity rate changes during the 1997 Umbria–Marche sequence (central Italy) through a rate-and-state dependent model, *J. Geophys. Res.*, 113, B11301, doi:10.1029/2007JB005356.
- Clarke P.J., Davies R.R., England P.C., Parsons B., Billiris H., Paradissis D., Veis G., Cross P. A., Denys P.H., Ashkenazi V., Bingley R., Kahle H. G., Muller M.V. and Briole P. 1998. Crustal strain in central Greece from repeated GPS measurements in the interval 1989–1997, *Geophys. J. Int.*, 135, 195– 214.
- Dieterich J.H. 1994. A constitutive law for rate of earthquake production and its application to earthquake clustering, *J. Geophys. Res.*, 99, 2601–2618.
- Dieterich J.H. and Kilgore B. 1996. Implications of fault constitutive properties for earthquake prediction, *Proc. Natl. Acad. Sci.*, 93, 3787–3794.
- Gomberg J., Bodin P. and Reasenberg P.A. 2003. Observing Earthquakes triggered in the near field by dynamic deformations, *Bull. Seismol. Soc. Am.*, 93, 118-138.
- Hatzfeld D. and Martin C. 1992. Intermediate depth seismicity in the Aegean defined by teleseismic data, *Earth Planet. Sci. Lett.*, 113, 267– 275.
- Kiratzi A.A. and Papazachos C.B. 1995. Active seismic deformation in the southern Aegean Benioff zone, *J. Geodynamics*, 19, 65-78.
- Leptokaropoulos K.M., Karakostas V.G., Papadimitriou E.E., Adamaki A.K., Tan O. and İnan S. 2013. A homogeneous earthquake catalogue compilation for western turkey and magnitude of completeness determination (*submitted manuscript*).
- McClusky S., Balassanian S., Barka A., Demir C., Ergintav S., Georgiev I., Gurkan O., Hamburger M., Hurst K., Kahle H., Kastens K., Kekelidze G., King R., Kotzev V., Lenk O., Mahmoud S., Mishin A., Nadariya M., Ouzounis A., Paradissis D., Peter Y., Prilepin M., Reilinger R., Sanli I., Seeger H., Tealeb A., Toksöz M. N. and Veis G. 2000. Global Positioning System constraints on plate kinematics and dynamics in the eastern Mediterranean and Caucasus, *J. Geophys. Res.*, 105, 5695-5719.

- Papadimitriou E.E. and Karakostas V.G. 2008. Rupture model of the great AD 365 Crete earthquake in the southwestern part of the Hellenic Arc, *Acta Geophys.*, 56, 293-312.
- Papazachos B. C. and Comninakis P.E. 1971. Geophysical and tectonic features of the Aegean Arc, *J. Geophys. Res.*, 76, 8517-8533.
- Papazachos B. C. 1996. Large seismic faults in the Hellenic Arc, *Annali Geof.*, 39, 891-903.
- Papazachos B.C. and Kiratzi A. 1996. A detailed study of the active crustal deformation in the Aegean and surrounding area, *Tectonophysics*, 253, 129–153.
- Papazachos B.C., Papadimitriou E.E., Kiratzi A.A., Papazachos C.B. and Louvari E.K. 1998. Fault plane solutions in the Aegean and the surrounding area and their tectonic implications, *Boll. Geof. Teor. Appl.*, 39, 199–218.
- Papazachos B.C., Karakostas B.G., Papazachos C.B. and Scordilis E.M. 2000. The geometry of the Benioff zone and lithospheric kinematics in the Hellenic Arc, *Tectonophysics*, 319, 275–300.
- Papazachos B.C. and Papazachou C. 2003. *The Earthquakes of Greece*, Ziti Publ., Thessaloniki, 317 pp.
- Papazachos C.B. and Nolet G. 1997. P and S deep velocity structure of the Hellenic Arc obtained by robust nonlinear inversion of travel times, *J. Geophys. Res.*, 102, 8349-8367.
- Scordilis E.M., Karakasis G.F., Karakostas B.G., Panagiotopoulos D. G., Comninakis P.E., and Papazachos B.C. 1985. Evidence for transform faulting in the Ionian Sea: The Cephalonia Island earthquake sequence, *Pure Appl. Geophys.*, 123, 388-397.
- Shaw, B., 2012. *Active tectonics of the Hellenic subduction zone*, Springer Theses, 169 pp.
- Silverman B.W. 1986. *Density Estimation for Statistic and Data Analysis*, Chapman and Hall, London, pp 9, 21.
- Simpson R.W. and Reasenberg P.A. 1994. Earthquake-induced static stress changes on central California faults, in the Loma Prieta, California earthquake of October 17, 1989 – *Tectonic processes, and models*, ed. Simpson R. W., U. S. Geol. Surv. Prof. Pap., 1550-F, F55–F89.
- Spakman W., Wortel M.J.R. and Vlaar N.S. 1988. The Hellenic subduction zone: a tomographic image and its geodynamic implications, *Geophys. Res. Lett.*, 15, 60-63.
- Taymaz T., Jackson J. and Westaway R. 1990. Earthquake mechanisms in the Hellenic trench near Crete, *Geophys. J. Int.*, 102, 695-731.
- Taymaz T., Jackson J. A. and McKenzie D. 1991. Active tectonics of the north and central Aegean Sea, *Geophys. J. Int.*, 106, 433–490.
- Toda S., Stein R. S., Reasenberg P. A. and Dieterich J. H. 1998. Stress transferred by the 1995 $M_w = 6.9$ Kobe, Japan, shock: Effect on aftershocks and future earthquake probabilities, *J. Geophys. Res.*, 103, 24, 543–24,565.
- Toda S. and Stein R.S. 2003. Toggling of seismicity by the 1997 Kagoshima earthquake couplet: A demonstration of time-dependent stress transfer, *J. Geophys. Res.*, 108, 2567, doi:10.1029/2003JB002527.
- Toda S., Stein R. S., Richards-Dinger K. and Bozkurt S. 2005. Forecasting the evolution of seismicity in southern California: Animations built on earthquake stress transfer, *J. Geophys. Res.*, 110, doi:10.1029/2004JB003415.
- Yolsal-Çevikbilen S. and Taymaz T. 2012. Earthquake source parameters along the Hellenic subduction zone and numerical simulations of historical tsunamis in the Eastern Mediterranean, *Tectonophysics*, 536-537, 61-100.